Angle-dependent Mössbauer spectroscopy in the ground and metastable electronic states in $Na_2[Fe(CN)_5NO]\cdot 2H_2O$ single crystals

Th. Woike and M. Imlau
Institut für Kristallographie, Universität zu Köln, Zülpicherstraße 49b, D-50674 Köln, Germany

V. Angelov
Department of Atomic Physics, Faculty of Physics, Sofia University, 5 James Bourchier Boulevard, 1164 Sofia, Bulgaria

J. Schefer and B. Delley
Paul Scherrer Institute, FUN Department, 5232 Villigen PSI, Switzerland
(Received 8 November 1999)

Upon excitation of the metastable electronic state *S*I by irradiation with light in the blue-green spectral range at temperatures below $T=200$ K the electron density in the $[Fe(CN)_5NO]^{2-}$ anion is rearranged mainly in the region of the Fe-N-O bonds, resulting in the drastic increase of the quadrupole splitting and a more positive isomer shift. But the local symmetry of the first coordination sphere around the Fe central atom is conserved. The positive sign of the electric-field gradient is unaffected by the new electron density at the ^{57}Fe central atom. The direction of the *z* component of the electric-field gradient with respect to the crystallographic *a* axis increases only by 0.4°. The degeneracy of the Fe($3d_{xz,yz}$) and Fe($4p_{x,y}$) orbitals is not changed. The optically excited anions are independent from each other and have no influence on the anions in the ground state. At every value of the population, the Mössbauer parameters of both states are not altered, only the number density of transfered anions is changed. These results are determined by measuring the sign and orientation α of the electric-field gradient, the asymmetry parameter η, the ^{57}Fe Debye-Waller factors f_a, f_b, f_c of the orthorhombic crystal and the mean-square displacement tensor in the ground and metastable state *S*I at $T=80$ K by angle dependent Mössbauer spectroscopy. Additionally these parameters are also determined at $T=294$ K for comparison. The dependence of the linewidth Γ on the crystal thickness, measured at $T=294$ K, yields again the Debye-Waller factors and at thickness zero the deviation from the natural linewidth Γ_N, given by the linebroadening of the γ source.

I. INTRODUCTION

For many years extremely long-living metastable electronic states, which can be excited by light, have been of fundamental interest for technological applications such as information or energy storage elements and for investigations of the correlation between electron density and structural properties in molecules and solids. They are suited for serial (bit-by-bit) and parallel (holographic) information storage, with extremely high capacity.[1,2] No external dopants or defects are needed for photorefractive behavior in holography.[3,4] An interesting kind of energy storage can be obtained, transforming the excited electron density into a charge transport by applying an external voltage. Since the electron density is changed upon optical excitation, Mössbauer spectroscopy provides a special tool for investigating structural as well as electronic properties and lattice dynamics with high accuracy. The Mössbauer nucleus is influenced by the excited electron density, which can be seen in the isomer shift (IS) and quadrupole splitting (QS). Rotating the sample with respect to the incoming γ beam, structural as well as electronic details and the mean-square displacement tensor can be obtained.

It is a lucky chance that such nearly infinitely long-living metastable electronic states discovered by Hauser, Oestreich, and Rohrweck[5] exist in the molecular ion $[Fe(CN)_5NO]^{2-}$, since $Na_2[Fe(CN)_5NO]\cdot 2H_2O$ (sodium nitroprusside, SNP) single crystals are used as a calibration standard for the velocity of the Mössbauer drive system.[6] Two metastable configurations (*S*I, *S*II) can be excited by irradiation with light in the spectral region of 350–580 nm at temperatures below 200 K (*S*I) and 150 K (*S*II). A maximum population of 50% of the anions in *S*I can be obtained with the wavelength (450 ± 10) nm and the polarization of the electric-field vector parallel to the crystallographic *c* axis ($\mathbf{E}\|c$) of the orthorhombic crystal. Polarization along the *a* or *b* axis yields a maximum of the population at (522 ± 5) nm with about 20%. Reversible recombination into the ground state (GS) is possible by irradiation with light in the spectral range of 600–900 nm or by heating above 150 K (*S*II) and 200 K (*S*I), respectively. The stability of the new states can be explained by the high activation energy of 0.68 eV (*S*I) and 0.52 eV (*S*II) with a frequency factor of about 5×10^{15} s^{-1}. They are lying energetically about 1 eV above the ground state.[7] The population is a linear one photon absorption process, starting from the occupied mainly $3d_{xz,yz}$ or $3d_{xy}$ crystal-field orbitals of the Fe central atom, exciting the empty antibonding π^*NO orbital of the NO ligand and then occupying the new states by a radiationless relaxation process. Analogous results are observed in a lot of Ru complexes like $K_2[RuCl_5NO]$, $K_2[Ru(CN)_5NO]$, $K_2[Ru(NO_2)_4(OH)(NO)]$, $[RuCl(en)_2NO]Cl_2$, $[RuBr(en)_2NO]Br_2$ and $[Ru(H_2O)(en)_2NO]Cl_3$.[8–10] Ra-

man and IR spectra combined with the Badger rule reveal an elongation of the Fe-N and N-O bonds in *S*I, which is confirmed by neutron and x-ray structural analysis.[11–13] The rearrangement of the electron density on the Fe central atom upon excitation of *S*I or *S*II is connected with new absorption bands in the red- and UV spectral range.[1] In all three states, GS, *S*I, and *S*II, single crystals of SNP are diamagnetic, as determined in EPR measurements[14,15] and through the temperature dependence of the quadrupole splitting,[16] so that no triplet or quintet state is excited. In contrast to the proposal of Güdel[17] and recent EPR results of Tritt-Goc,[18] no low spin–high spin transition takes place and no free spin density could be found on the central Fe atom. Recently, Carducci, Pressprich, and Coppens[19] have proposed on the basis of x-ray analysis that the metastable state *S*I is formed by rotation of the N-O ligand:

(GS): Fe-N-O $\rightarrow$(*S*I): Fe-O-N

The main argument is the large mean-square displacement of the oxygen atom, which can be reduced after the rotation of the N-O ligand. The energetic stability of the Fe-O-N configuration could be demonstrated by density-functional calculations,[20] in which the Mössbauer parameters QS, IS, and η of GS and *S*I can be reproduced with sufficient accuracy. However, contrary to this calculation, a hyperfine splitting (triplet) could be found in the EPR spectra after preexposure with x rays and subsequent irradiation with blue light at $T=80$ K,[14,15] producing formally Fe($3d^7$). This triplet state results from the coupling of the free electron spin on the Fe($3d^7$)-central atom with the nuclear spin $S=1$ of ^{14}N, which would be impossible, if the Fe-O-N configuration (inversion) existed. Because of all these partly contradictory results and interpretations, it is necessary to obtain more structural details, more information about the electron density around the Fe central atom and about the vibrational behavior of the Fe atom in the anion. Therefore in this article we have analyzed the following properties of the ground and metastable state *S*I by angle dependent Mössbauer spectroscopy:

(i) structural conditions by measuring the direction of the electric-field gradient (EFG) with respect to the crystallographic *a* axis;

(ii) the electron density around the Fe central atom, given by QS and IS, the asymmetry parameter η and the sign of the EFG;

(iii) lattice dynamic and vibrational behavior of the Fe atom detected by the Debye-Waller factors and the direction of the principal axis of the mean-square displacement tensor (MSD) with respect to the crystallographic *a* axis.

II. EXPERIMENTAL DETAILS

Deep red single crystals of SNP with high optical quality and dimensions of $100\times50\times50$ mm^3 can be grown by slow evaporation at temperatures of 320 K. Orientated crystal plates (100), (010), and (001) were cut, ground with a mixture of Al_2O_3 and propanol to the desired thickness and finally etched with a mixture of propanol and water (3:1). The Mössbauer source ^{57}Co[Rh] of about 40 mCi activity was moved with constant acceleration by an electromagnetic vibrator. The linewidth Γ_s [full width at half maximum (FWHM)] of the source was determined by measuring the thickness dependence of *a*, *b*, and *c* cuts at room temperature. Extrapolating the sum of the absorber and source linewidth ($\Gamma_A+\Gamma_S$) to thickness zero, we obtain Γ_S by three independent series of measurements, assuming that $\Gamma_A=\Gamma_N$, whereby Γ_N is the natural linewidth. The γ quanta are detected with a NaI(Tl) scincillator of 0.1 mm thickness. The temperature of the source was kept constant at (294 ± 0.7) K and that of the absorber at (294 ± 0.7) K and at (80 ± 1) K. The temperature dependence of the crystal thickness and density was considered by measuring the thermal expansion along the *a*, *b*, and *c* axis. The samples were fixed on a copper-gold finger with silver paste inside a vacuum cryostat. At 80 K the vacuum was better than 10^{-6} Torr. At room temperature the crystals are at normal pressure due to the lack of crystal water at about 10^{-2} Torr. The cold finger could be rotated with an angle accuracy of $\pm0.1°$. The diameter of the sample was $d=6$ mm. The distance between source and detector was 40 cm, so that the aperture of the γ beam is 0.5°. Every sample was rotated from $+50$ to $-50°$, so that an angle overlap exists between the crystals of *a* and *b* cut by rotation around the *c* axis. The population of *S*I was performed with an Ar^+ laser, using the wavelength $\lambda=457.9$ nm, in order to get a population of about 50% by irradiation with the electric-field vector *E* parallel to the *c* axis of the *a* or *b* cut. The *c* cut was irradiated with $\lambda=514.5$ nm to reach a population of about 18 % with $\mathbf{E}\|a$ or *b* axis. The background corrections of the line intensities were measured with the *black filter* technique. The black filter consists of ^{57}FeOOH (14 mg/cm^2), embedded in polyvenylalcohol, placed in front of the detector. Two measurements are necessary for the background corrections:

(i) Source and black filter moving with high velocity, $v=\infty$, so that all γ quanta from the source can be detected (resonant and nonresonant), which yields the counts $N(\infty)$.

(ii) Source and black filter are at rest, $v=0$ mm/s, so that only γ quanta with recoil are detected, yielding the counts $N(0)$.

Taking the recoilless absorption of the black filter ($\epsilon=0.96$) into account when it is at rest with respect to the source, we obtain the recoilless part of the γ quanta in the window of the differential discriminator β form,

$$\beta=\frac{N(\infty)-N(0)}{N(\infty)\cdot\epsilon}. \tag{2.1}$$

With β we can separate the recoilless and nonrecoilless parts in the measured Mössbauer spectra. β was determined twice per day. More details about the black filter are given in Ref. 21. With this result we can determine the Debye-Waller factors f_a, f_b, and f_c of the GS with respect to the crystallographic *a*, *b*, and *c* axes. For the calibration of our spectrometer we have taken the value of the quadrupole splitting from Ref. 22, QS$=1.7034$ mm/s at room temperature. Every spectrum is evaluated using the transmission integral procedure described in the Appendix. The accumulated counts of every spectrum were always higher than 10^6 counts/channel, so that the statistical error can be neglected in the discussion of our results. In order to obtain an estimate of the quality of every single spectrum, we have calculated, from more than 30 single spectra for one angle dependent measurement, the $\pm3.6\cdot\sigma$ error bars for every determined parameter, whereby

σ denotes the standard deviation. Every single spectrum lies within this error region, indicated by the error bars in the corresponding figures.

III. STRUCTURAL AND THEORETICAL CONSIDERATIONS

Structural details have to be known for angle dependent measurements and calculations of the cross sections. A complete structural analysis of SNP was performed in 1965 by Manoharan and Hamilton.[23] In the theoretical part we derive all effective thicknesses and polarization factors for our evaluation, starting from the basic work of Grant, Housley, and Gonser.[30] We discuss their sensitivity by varying the significant parameters.

A. Structural details

SNP crystallizes in the orthorhombic space group *Pnnm* with four molecules per unit cell. As a consequence of the inversion symmetry, the $[Fe(CN)_5NO]^{2-}$ anions lie in couples in the *a-b*-mirror plane in antiparallel directions with their quasifourfold N-C-Fe-N-O axes. Structural data are taken from Ref. 11, measured at 80 K. Data at room temperature are given in Refs. 24 and 25, at 150 K in Ref. 26, at 138 K in Ref. 13, and at 50 K in Ref. 19. The morphology of the single crystal is shown in Fig. 1(a). The natural grown (001) face is important and allows a precise preparation of the crystallographic *a* and *b* plates. Both optical axes are lying in the (101) and $(10\bar{1})$ faces. The optical character of SNP is 2^-. The anion with quasi-4*m* symmetry is drawn in Fig. 1(b).[11] The Fe central atom is surrounded in the first coordination sphere by five carbon and one nitrogen atoms. The symmetry of the fourfold axis is broken by the C1-Fe-N4 angle (176.7°) and the Fe-N4-O1 angle (176.1°). A small difference between the equivalent Fe-C and C-N bond lengths exists. The unit cell with only two anions is drawn in Fig. 1(c). The quasifourfold axis of the anions, symbolized by arrows, are shown, in order to elucidate the two orientations of the anions in the *a-b* mirror plane, so that two groups of anions (1,2) have to be considered. The angle ϕ_C is formed by the C1-Fe axis trans to the N4-O1 ligand and the angle ϕ_N by the Fe-N4 axis with respect to the crystallographic *a* axis. At room temperature their values are: $\phi_C = 37.48°$, $\phi_N = 34.28°$, measured by x-ray[24] and $\phi_C = 37.38°$, $\phi_N = 34.12°$ detected by neutron diffraction.[25] These angles can be compared with the direction of the EFG in GS, discussed below. As shown in Fig. 1(c), the propagation vector $\mathbf{k}_\gamma$ of the 14.41 keV γ quanta determines the rotation angle Ω with the *a* and *b* axes starting at $\Omega = 0°$ for $\mathbf{k}_\gamma \| a$ axis. The measurement of $\mathbf{k}_\gamma \| c$ axis is a special case, in which the propagation of $\mathbf{k}_\gamma$ lies always perpendicular to the *a-b* mirror plane. In this case one cannot decide between the two groups of anions. The polarization directions of the γ quanta, coming from an unpolarized source, are denoted by $\mathbf{e}_1$ and $\mathbf{e}_2$. The whole lattice is built up by the crystal water and the Na^+ cations, which are connected to the anions via the negative $(C\text{-}N)^-$ ligands. The shortest ligand-cation distance has an amount of 249.0 pm, formed by the axial $(C1\text{-}N1)^-$ ligand and the Na^+ cation. The distance between equatorial $(C\text{-}N)^-$ and Na^+ is 249.8 and 250.8 pm. Because of these distances the Na^+ cations have considerable influence on the amount of the EFG of the Fe central atom by polarization of the 3*d*, 4*p* electron density via the $(C\text{-}N)^-$ ligands. This effect is confirmed by the difference of QS in

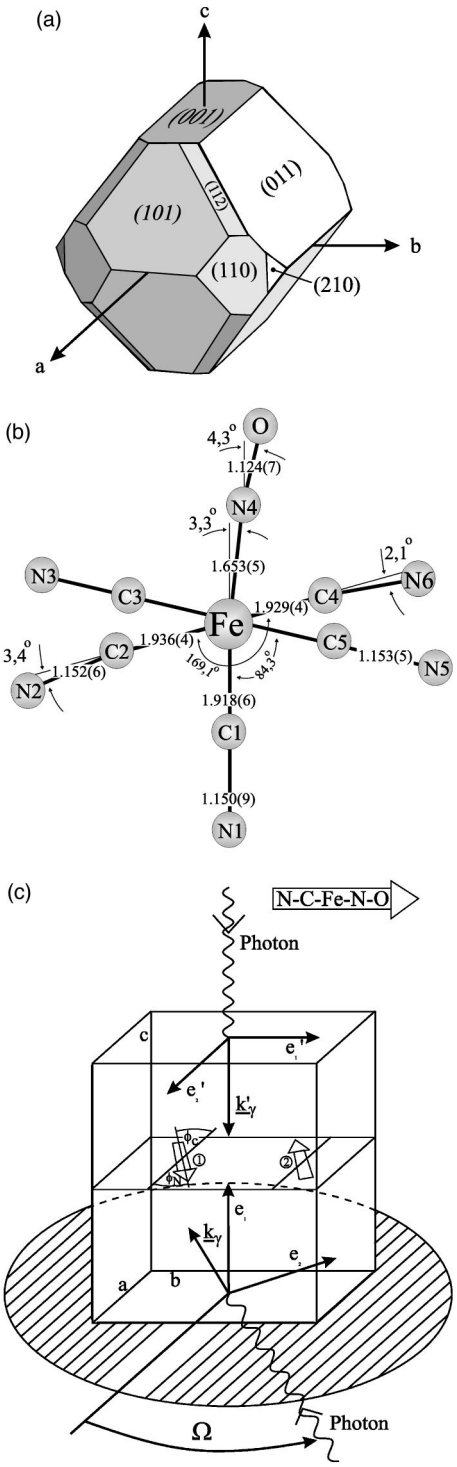

FIG. 1. Details of the structure and symmetry of $Na_2[Fe(CN)_5NO]\cdot 2H_2O$. (a) Morphology of the grown crystal. (b) The $[Fe(CN)_5NO]^{2-}$ anion in the ground state. The atomic distances are given in Å. (c) Unit cell with only two positions of the anions. Drawn are the N-C-Fe-N-O quasifourfould axes symbolized by arrows. 1,2 determine the two groups of anions, and Ω is the rotation angle lying in the $a-b$ mirror plane. The angles ϕ_c, ϕ_n are formed by the C1-Fe and Fe-N4 directions, respectively, with respect to the *a* axis.

structural equivalent cation substituted nitroprusside like $Li_2[Fe(CN)_5NO]\cdot 4H_2O$, (space group $Pnnm$, $Z=4$) where QS = 1.86 mm/s at room temperature,[27] compared to 1.7034 mm/s for SNP,[22] so that a precise calculation of QS has to consider such a polarization effect, which exceeds QS of SNP by about 9%.

B. Theoretical details

The electric-field gradient $q=V_{zz}/e$ can be determined by measuring the quadrupole splitting QS, knowing the nuclear quadrupole moment Q, calculated recently in Ref. 28, and the asymmetry parameter η:

$$QS=\frac{e^2Q}{2}q\sqrt{1+\frac{\eta^2}{3}}, \tag{3.1}$$

where e is the electron charge, q is the EFG, and η is defined as $\eta=(V_{xx}-V_{yy})/V_{zz}$, with $|V_{xx}|\leqslant|V_{yy}|\leqslant|V_{zz}|$, so that $0\leqslant\eta\leqslant 1$, and the second derivatives of the potential V_{xx}, V_{yy}, V_{zz} are the components of the diagonalized EFG tensor. An accurate determination of η can be performed by angle dependent measurements, which also reveal the sign of q and in addition in SNP the direction of V_{zz} with respect to the crystallographic a axis, denoted by the angle α as orientation parameter. Emission of an unpolarized source consists of two independent polarization directions of γ quanta with equal intensity as depicted in Fig. 1(c). In a single crystal, however, the absorption lines of a quadrupole doublet have polarization dependent cross sections, which are sensitive to the angle of incidence of the γ quanta, with respect to the direction of the EFG. In many articles, the angle dependence of the area of the Mössbauer lines and the polarization dependent cross sections are discussed for the ground state of SNP.[29–35] Grant, Housley, and Gonser[30] have calculated these cross sections and they have determined α, η, ω, f_a, f_b, f_c as defined below at room temperature by measuring at four different angles. In the following, we will explicitly evaluate, on the basis of Ref. 30, the effective thicknesses $t_{1/2}$, $t_{3/2}$, and all equations, which we have used in order to determine α, η, ω, f_a, f_b, f_c and the fractional polarizations $a_{1/2}$, $a_{3/2}$. The evaluation of the measured spectra by the transmission integral procedure and the self-consistent iteration algorithm for the determination of all above given parameters are presented in the Appendix.

C. $\mathbf{k}_\gamma$ lying in the a-b-mirror plane

The cross section σ is given by the 2×2 density matrix

$$\sigma=\begin{vmatrix}\sigma_{11}\sigma_{21}\\ \sigma_{12}\sigma_{22}\end{vmatrix}. \tag{3.2}$$

Upon transformation on EFG main axes and from there into the crystallographic system the following equations for the two groups of anions 1 and 2 shown in Fig. 1(b) are obtained:[30]

$$\sigma_{11}^1=\frac{1}{2}\sigma_o f_1\left[\frac{1}{2}\pm\frac{1}{4}\sqrt{\frac{3}{3+\eta^2}}\cdot(1-\eta)\right];\quad \sigma_{12}^1=\sigma_{21}^1=0, \tag{3.3}$$

$$\sigma_{11}^2=\frac{1}{2}\sigma_o f_2\left[\frac{1}{2}\pm\frac{1}{4}\sqrt{\frac{3}{3+\eta^2}}\cdot(1-\eta)\right];\quad \sigma_{12}^2=\sigma_{21}^2=0, \tag{3.4}$$

$$\sigma_{22}^1=\frac{1}{2}\sigma_o f_1\left[\frac{1}{2}\pm\frac{1}{4}\sqrt{\frac{3}{3+\eta^2}}\cdot[1-3\sin^2(\Omega-\alpha)+\eta\cos^2(\Omega-\alpha)]\right], \tag{3.5}$$

$$\sigma_{22}^2=\frac{1}{2}\sigma_o f_2\left[\frac{1}{2}\pm\frac{1}{4}\sqrt{\frac{3}{3+\eta^2}}\cdot[1-3\sin^2(\Omega+\alpha)+\eta\cos^2(\Omega+\alpha)]\right]. \tag{3.6}$$

The negative sign describes the $\pm 1/2\rightarrow\pm 1/2$ and the positive sign the $\pm 1/2\rightarrow 3/2$ nuclear transition, respectively. $\sigma_0=2.57\times 10^{-18}$ cm^2 is the nuclear cross section for resonant absorption and f_1, f_2 are the ^{57}Fe Debye-Waller factors of the two groups of anions, Ω is the rotation angle of the sample between $\mathbf{k}_\gamma$ and the crystallographic a axis given in Fig. 1(c). The average cross sections σ^1, σ^2 and fractional polarizations $a_{1/2}$, $a_{3/2}$ are defined as

$$\sigma^1=\frac{1}{2}(\sigma_{11}^1+\sigma_{22}^1)=\frac{1}{4}\sigma_o f_1(1\pm A_1),$$

$$A_1=\frac{1}{4}\sqrt{\frac{3}{3+\eta^2}}\cdot[2-(3+\eta)\sin^2(\Omega-\alpha)], \tag{3.7}$$

$$\sigma^2=\frac{1}{2}(\sigma_{11}^2+\sigma_{22}^2)=\frac{1}{4}\sigma_o f_2(1\pm A_2),$$

$$A_2=\frac{1}{4}\sqrt{\frac{3}{3+\eta^2}}\cdot[2-(3+\eta)\sin^2(\Omega+\alpha)], \tag{3.8}$$

$$a_{1/2,3/2}=\left.\frac{\sigma_{11}^1-\sigma_{22}^1+\sigma_{11}^2-\sigma_{22}^2}{\sigma_{11}^1+\sigma_{22}^1+\sigma_{11}^2+\sigma_{22}^2}\right|_{1/2,3/2}. \tag{3.9}$$

The indices 1/2 and 3/2 denote the transitions $\pm 1/2\rightarrow\pm 1/2$ and $\pm 1/2\rightarrow\pm 3/2$, respectively. The effective thickness t is given by $t=n_A\cdot\sigma$, whereby n_A is the number of ^{57}Fe nuclei per cm^2. Therefore

$$t_{1/2}=n_A(\sigma_{11}^1+\sigma_{22}^1+\sigma_{11}^2+\sigma_{22}^2)|_{1/2}, \tag{3.10}$$

$$t_{3/2}=n_A(\sigma_{11}^1+\sigma_{22}^1+\sigma_{11}^2+\sigma_{22}^2)|_{3/2}. \tag{3.11}$$

The ratio $t_{1/2}/t_{3/2}$ of the effective thicknesses is a function of the rotation angle Ω and depends on the parameters α, η, and $g=f_1/f_2$:

$$\frac{t_{1/2}}{t_{3/2}}=\frac{2(\sigma^1+\sigma^2)|_{1/2}}{2(\sigma^1+\sigma^2)|_{3/2}}=\frac{2\cdot(g+1)}{g\cdot(1+A_1)+(1+A_2)}-1 \tag{3.12}$$

in which

$$g=\frac{f_1}{f_2}=\exp(-G_o\cdot\sin 2\Omega) \tag{3.13}$$

and

$$G_o=k_\gamma^2(\langle z^2\rangle-\langle y^2\rangle)\cdot\sin 2\omega. \tag{3.14}$$

Here, ω is the angle between the main axis of the mean-square displacement tensor (MSD) and the crystallographic a axis and $k_\gamma^2=5.334\times10^{17}$ cm^{-2} is the square of the wave vector of the γ quanta. If the electric-field vector of the light vibrates during the population parallel to the crystallographic c axis (perpendicular to the mirror plane m) the two groups of anions are equally excited, so that the number of excited anions n_1, n_2 are the same ($n_1/n_2=1$) and this ratio is not considered in Eq. (3.12). $\langle z^2\rangle$ and $\langle y^2\rangle$ are the MSD's of the ^{57}Fe nucleus in the coordinate system of the anions. The z and y coordinates are lying in the a-b mirror plane, z is defined by the N1-C1-Fe direction and y is perpendicular to z. Upon transformation into the crystallographic system we obtain

$$G_o=k_\gamma^2(\langle a^2\rangle-\langle b^2\rangle)\cdot\tan 2\omega. \tag{3.15}$$

The MSD's $\langle a^2\rangle$ and $\langle b^2\rangle$ are received by measuring with $\mathbf{k}_\gamma$ parallel to the a and b axis, respectively. In this case, considering the small line broadening, the sum of the effective thicknesses is

$$t_{1/2}+t_{3/2}|_a=n_A\sigma_o f_a\frac{\Gamma_N}{\Gamma_A}, \tag{3.16}$$

$$t_{1/2}+t_{3/2}|_b=n_A\sigma_o f_b\frac{\Gamma_N}{\Gamma_A} \tag{3.17}$$

from which we obtain the MSD's by

$$\langle a^2\rangle=-\ln(f_a/k_\gamma^2)\ \text{ and }\ \langle b^2\rangle=-\ln(f_b/k_\gamma^2) \tag{3.18}$$

if n_A and Γ_A are known. The polarization factors $a_{1/2}$ and $a_{3/2}$ can also be calculated from the cross sections

$$a_{1/2}=-\frac{(g+1)\cdot W-(L_1g+L_2)}{(g+1)\cdot(1-W)-(L_1g+L_2)}, \tag{3.19}$$

$$a_{3/2}=-\frac{(g+1)\cdot W-(L_1g+L_2)}{(g+1)\cdot(1+W)+(L_1g+L_2)} \tag{3.20}$$

with the abbreviations

$$W=\frac{1}{4}\sqrt{\frac{3}{3+\eta^2}}(1-\eta), \tag{3.21}$$

$$L_1=\frac{1}{4}\cdot\sqrt{\frac{3}{3+\eta^2}}\cdot[1-3\sin^2(\Omega-\alpha)+\eta\cos^2(\Omega-\alpha)], \tag{3.22}$$

$$L_2=\frac{1}{4}\cdot\sqrt{\frac{3}{3+\eta^2}}\cdot[1-3\sin^2(\Omega+\alpha)+\eta\cos^2(\Omega+\alpha)]. \tag{3.23}$$

The polarization factors depend on α, η, and G_0 in an equivalent way as the effective thicknesses. The self-consistent iteration algorithm for the calculation of $t_{1/2}$ and $t_{3/2}$ together with $a_{1/2}$ and $a_{3/2}$ is given in the Appendix. The area of every Mössbauer line in our spectrum is composed by the cross sections of the two groups of anions in the effective thickness and the fractional polarization.

D. $\mathbf{k}_\gamma\|$ c axis (perpendicular to the a-b mirror plane)

In this special case the cross sections are the same for the two groups of molecules and $f_1=f_2=f$:

$$\sigma_{11}^1=\sigma_{11}^2=\frac{1}{2}\sigma_o f\left[\frac{1}{2}\pm\frac{1}{4}\sqrt{\frac{3}{3+\eta^2}}[1-3\sin^2\alpha+\eta\cos^2\alpha]\right], \tag{3.24}$$

$$\sigma_{22}^1=\sigma_{22}^2=\frac{1}{2}\sigma_o f\left[\frac{1}{2}\pm\frac{1}{4}\sqrt{\frac{3}{3+\eta^2}}[1-3\cos^2\alpha+\eta\sin^2\alpha]\right], \tag{3.25}$$

$$\sigma_{12}^1=\sigma_{12}^2=\sigma_{21}^1=\sigma_{21}^2=0. \tag{3.26}$$

The ratio $t_{1/2}/t_{3/2}$ is only a function of η:

$$\frac{t_{1/2}}{t_{3/2}}=\frac{1+\frac{1}{4}\sqrt{\frac{3}{3+\eta^2}}(1-\eta)}{1-\frac{1}{4}\sqrt{\frac{3}{3+\eta^2}}(1-\eta)}. \tag{3.27}$$

Again from the sum of the effective thicknesses $t_{1/2}+t_{3/2}$ the Debye-Waller factor f_c and the mean-square displacement $\langle c^2\rangle$ can be determined:

$$t_{1/2}+t_{3/2}|_c=n_A\sigma_0 f_c\frac{\Gamma_N}{\Gamma_A}, \tag{3.28}$$

$$\langle c^2\rangle=-\ln(f_c/k_\gamma^2). \tag{3.29}$$

The polarization factors, however, depend on η and α, but not on ω and Ω:

$$a_{1/2,3/2}=\frac{\pm\frac{1}{4}\sqrt{\frac{3}{3+\eta^2}}(3+\eta)(\sin^2\alpha-\cos^2\alpha)}{1\pm\frac{1}{4}\sqrt{\frac{3}{3+\eta^2}}(\eta-1)}. \tag{3.30}$$

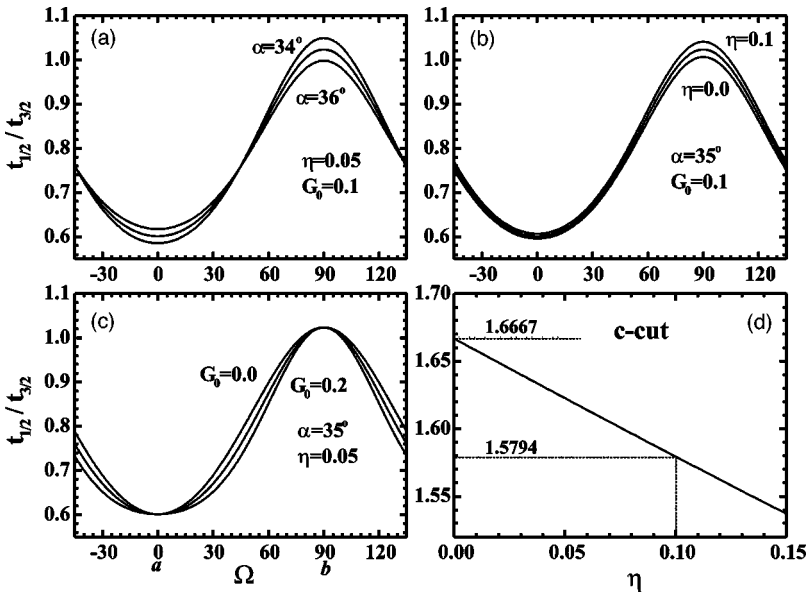

FIG. 2. Sensitivity of the angle dependent Mössbauer spectroscopy for the parameters α, η, G_o. (a) Variation of α from 34 to 36°, $\eta=0.05$ and $G_0=0.1$ are fixed. (b) Variation of η from 0.0 to 0.1, $\alpha=35°$, and $G_0=0.1$ are fixed. (c) Variation of G_0 from 0.0 to 0.2, $\alpha=35°$ and $\eta=0.05$ are fixed. (d) Dependence of $t_{1/2}/t_{3/2}$ on η in the *c*-cut direction.

Obviously, *w* cannot be determined from this special direction. There exists no polarization effect at $\alpha=45^o$, which, however, is not the case in SNP. The sensitivity of $t_{1/2}/t_{3/2}(\Omega)$ with respect to the three parameters α, η, and G_0 can be demonstrated by varying one of them, using Eq. (3.12) as given in Figs. 2(a)–(c). In addition, Fig. 2(d) shows the dependence of $t_{1/2}/t_{3/2}$ on η for the special case of $\mathbf{k}_\gamma \| c$ axis, in the range of $0 \leqslant \eta \leqslant 0.15$. In the *a* and *b* cut the ratio $t_{1/2}/t_{3/2}$ lies between 0.6 and 1.0. If the sign of the EFG is positive the lower value 0.6 is reached with $\mathbf{k}_\gamma \| a$ axis, so that the sign of the EFG can be determined unambiguously by angle dependent measurements. The maximum sensitivity of $t_{1/2}/t_{3/2}$ for α and η occurs at $\Omega=90°$ and for G_0 at $\Omega=45°$. In Fig. 2(a), α is varied only from 34 to 36° with constant $\eta=0.05$ and $G_0=0.1$, whereby at $\Omega=90°$ the ratio $t_{1/2}/t_{3/2}$ decreases from 1.042 to 0.98 by 6%. In Fig. 2(b) the asymmetry parameter is changed from $\eta=0.1$ to $\eta=0$ with constant $\alpha=35°$ and $G_0=0.1$ and $t_{1/2}/t_{3/2}$ decreases from 1.041 to 1.005 by 3.5%. In Fig. 2(c), the parameter G_0 is varied from 0.0 to 0.2, and $\alpha=35°$ and $\eta=0.05$ are fixed. At $\Omega=45°$ the ratio $t_{1/2}/t_{3/2}$ decreases by 7%. An interesting fact is that $t_{1/2}/t_{3/2}$ depends in a different way on Ω for all three parameters. The ratio $t_{1/2}/t_{3/2}$ does not depend on α at $\Omega=45°$, it varies over the whole rotation range for η and is constant at $\Omega=0°$ and $\Omega=90°$ for G_0. These different behaviors guarantee a clear and distinct evaluation of α, η, and G_0. The special case of $\mathbf{k}_\gamma \| c$ axis is drawn in Fig. 2(d), in which $t_{1/2}/t_{3/2}$ depends only on η. If $\eta=0$ the ratio of the effective thickness is $t_{1/2}/t_{3/2}=1.6667$ and for $\eta=0.1$ we get $t_{1/2}/t_{3/2}=1.5794$. Such a decrease of 5.2% can easily be detected, especially in comparison between GS and *S*I, because both states are simultaneously in one and the same spectrum. However, the evaluation of η with $\mathbf{k}_\gamma \| c$ axis results only from one spectrum. Therefore we have taken it as a separate determination of η.

E. Thickness dependence of the linewidth Γ

The linear dependence of the linewidth Γ on the crystal thickness is restricted to the range of the effective thickness *t* of $0 \leqslant t \leqslant 4$. The general formula for SNP with $t=t_{1/2}+t_{3/2}$ is

$$\Gamma_i(t)=(\Gamma_S+\Gamma_A)+\Gamma_A \cdot C_i \cdot t_i, \quad (i=a,b,c). \tag{3.31}$$

Γ_S and Γ_A are the FWHM of the source and absorber, respectively, C_i depends on the polarization factors $a_{1/2}$ $a_{3/2}$, and t_i is the effective thickness, given by

$$t_i=(L \cdot d \cdot \rho/M) \cdot n_{Fe-57} \cdot \sigma_o \cdot f_i \cdot \Gamma_N/\Gamma_A. \tag{3.32}$$

L is the Avogadro number, $n_{Fe-57}=0.0214$ the natural abundance of ^{57}Fe, $\rho=1.7247(4)$ g/cm^3 the density of SNP at $T=297$ K, $M=297.955$ g/mol, d is the thickness of the crystal, and $\Gamma_N=0.0972$ mm/s the natural linewidth. Varying the thickness d, we get from the slope the Debye-Waller factors f_i and by extrapolating to thickness zero the sum $(\Gamma_S+\Gamma_A)$, which, in principle, has the value of $2\Gamma_N$. A small deviation is given by the line broadening of the source. For the two line absorber SNP, the linewidth is $\Gamma=1/2(\Gamma_{1/2}+\Gamma_{3/2})$. Correction for possible scattering processes are not considered. The constants C_i $(i=a,b,c)$ are calculated by the procedure of the transmission integral, given in the Appendix, so that the different polarizations for *a*, *b*, and *c* axis are taken into account. Using the known effective thicknesses and fractional polarizations from the rotation spectra we have produced simulated Mössbauer spectra for the dependence of $\Gamma(t_i)$ and from this linear slope we can calculate the parameters C_i. We have taken α, η, ω, and f_i from Table I calculating with the transmission integral simulated spectra, from which we have taken Γ and *t* for different thicknesses. The linear slope of $\Gamma(t)$ gives with the corresponding $a_{1/2}, a_{3/2}$ the parameters C_i.

However, the differences are very small: $C_a=0.270$, $C_b=0.286$, and $C_c=0.269$.

IV. EXPERIMENTAL RESULTS

The temperature shift of QS and IS in GS and *S*I is extensively discussed in Ref. 16. The main result is the fact that SNP remains diamagnetic in *S*I, due to the very small temperature dependence of QS. Furthermore, the normalized behavior of QS is the same for GS and *S*I and the difference of both isomer shifts (GS, *S*I) is constant over the whole tem-

TABLE I. Comparison of the evaluated Mössbauer parameters detected at $T=294$ K with recent measurements.

	This work	Ref. 27	Ref. 19
sign (q)	+	+	+
α	35.8(1)°	36.6(6)°	
η	0.02(1)	0.01(1)	
η_c	0.03(2)		
ω	14(6)°	1(7)°	
f_a	0.38(1)	0.367(2)	0.36(1)
f_b	0.35(1)	0.332(4)	0.33(1)
f_c	0.39(1)	0.377(4)	0.38(1)
$\delta\Omega_a$	1.2(3)°		
$\delta\Omega_b$	0.7(3)°		

perature range, which is a clear demonstration of a pure quadratic Doppler shift. Consequently, the *s*-electron density at the Fe nucleus decreases, but not due to any screening effect of the *d*-electron density. QS increases from QS=1.7034 mm/s at $T=297$ K (Ref. 22) to QS=1.716(3) mm/s at $T=80$ K and to QS=2.755(3) mm/s in *SI* at $T=80$ K.[37] Fixing IS to zero in the GS at $T=80$ K, IS increases to +0.178(3) mm/s in *SI* and the linewidths are broadened in *SI* at thickness zero by 1.4% with respect to GS.[37] These results are considered for the evaluation of our spectra.

A. Angle dependence at $T=294$ K

The ratio $t_{1/2}/t_{3/2}$ of the effective thickness as a function of the observation angle Ω in the *a*-*b* plane is shown in Fig. 3(a), and the corresponding polarization factors $a_{1/2}, a_{3/2}$ are plotted in Fig. 3(b), calculated by Eqs. (3.12), (3.19), (3.20), and the iteration procedure, given in the Appendix. The minimum value $t_{1/2}/t_{3/2}=0.617$ lies at $\mathbf{k}_\gamma \| a$ axis and the maximum value $t_{1/2}/t_{3/2}=0.989$ is reached at $\mathbf{k}_\gamma \| b$ axis. The fractional polarizations $a_{1/2}, a_{3/2}$ are nearly identical at $\Omega=90°$ with an amount of about 0.5. At $\Omega=0°$ they differ by a factor of 1.7, whereby $a_{1/2}=0.34$ and $a_{3/2}=0.2$. Due to the angle α the polarization behavior of SNP is not very pronounced. If $\alpha=\eta=0$, which is the case in $(CN_3H_6)_2[NP]$, we get at $\Omega=0°$: $a_{1/2}=a_{3/2}=0$ and $\Omega=90°$: $a_{1/2}=3/5$ and $a_{3/2}=3/7$. Using Eq. (3.12) and our iteration technique we obtain the parameters α, η, G_0. The Debye-Waller factors are calculated according to Eqs. (3.16) and (3.17) using $\Gamma_A=\Gamma_N$. From the measurements of $\mathbf{k}_\gamma \| c$ axis we have separately determined f_c and η, using the Eqs. (3.27) and (3.28). The fractional polarization factors $a_{1/2}$ and $a_{3/2}$ depend on α and η, so that we have taken α from above. All parameters are summarized together with those of Grant, Housley, and Gonser[30] and our recent measurements[21] in Table I. Additionally, we have determined η_c from the *c*-cut crystal, which coincides with η within the error limits. The deviation of the prepared *a*- and *b*-cut crystal plates from the ideal (100) and (010) faces in the *a* and *b* direction can be calculated utilizing the symmetry condition of Eq. (3.12), that the maximum and minimum of the rotation curve lie exactly at $\Omega=90°$ and $\Omega=0°$, respectively. These errors, produced by cutting and preparing the crystal plates, are given as $\delta\Omega_a$ and $\delta\Omega_b$. We cannot obtain such an error in the *c* direction, since the (001) face is a natural grown face, which can be precisely cut.

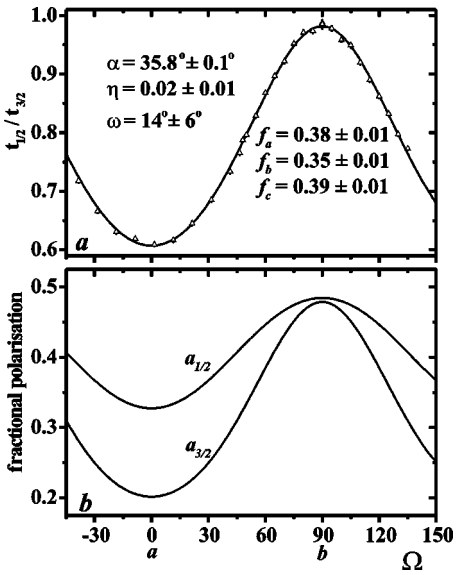

FIG. 3. (a) Angle dependence of $t_{1/2}/t_{3/2}$ at $T=294$ K. (b) Angle dependence of the fractional polarizations $a_{1/2}$ and $a_{3/2}$ at $T=294$ K.

The errors written in brackets are given as plus-minus values. The differences of the Debye-Waller factors show that they can be reproduced with an accuracy of about 5%. However, the data of Grant, Housley, and Gonser[30] are calculated from only four single spectra at four angles in the *a*-*b* plane, which leads to an underestimation of the errors and to an uncorrect value of ω due to the nearly identical Debye-Waller factors f_a and f_b. In order to determine the accuracy with which we can really determine the Debye-Waller factors using the black absorber technique, we have determined with a second independent measurement f_a, f_b, and f_c by the thickness dependence of the linewidth. The linear slopes of the *a*, *b*, and *c* cuts are shown in Fig. 4.

The effective thicknesses lie in the range of $0<t<3.6$, so that the linear relation of Eq. (3.31) is valid.[36,38] By extrapolating to thickness 0, the sum of Γ_S and Γ_A is given as 0.22(1), 0.24(2), and 0.22(1) mm/s for the *a*, *b*, and *c* cut, respectively. Assuming that the absorber has natural linewidth $\Gamma_A=\Gamma_N$ the source line is broadened by about 14%, which is typical for good sources. The Debye-Waller factors $f_a=0.37(1)$, $f_b=0.34(1)$, $f_c=0.38(1)$ are calculated using Eq. (3.31) with the parameters $C_a=0.270$, $C_b=0.286$, $C_c=0.269$. They are in good agreement with our present and earlier results given in Ref. 21. We have calculated $f=0.37(1)$ from the powder spectrum and get $\langle f\rangle=0.36(1)$ from the mean value of the data given above which is again in good agreement with the earlier data. The sign of the EFG is positive and the orientation parameter has an amount of $\alpha=35.8(1)°$. Since f_a and f_b are not very different from each other, the projection of the MSD tensor into the *a*-*b* plane is nearly a circle which explains the large error of ω and the difference between our results and that of Grant, Housley, and Gonser.[30] The directions of the EFG and the main axis of the MSD tensor do not coincide.

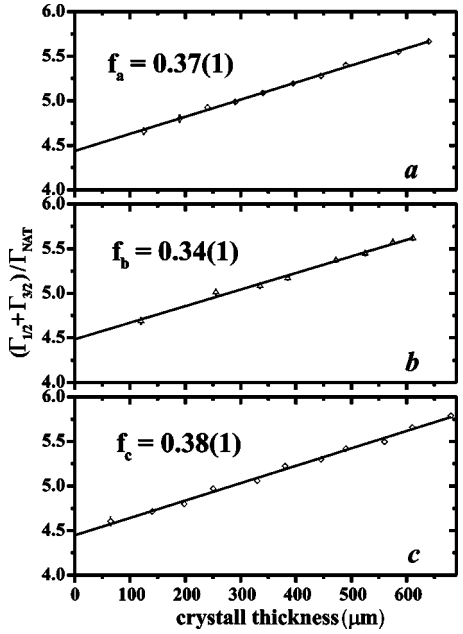

FIG. 4. Linear dependence of Γ on the crystal thickness at $T=294$ K for the *a*, *b*, and *c* cut.

B. Angle dependence at $T=80$ K for GS and *S*I

The Mössbauer spectra of GS and *S*I at $T=80$ K for *a*-, *b*-, and *c*-cut crystals are shown in Fig. 5. The dotted lines represent the curves fitted with the quadrupole splittings, the evaluated populations and the isomer shift of *S*I with respect to GS as inputs. The angle dependence of the cross sections can be seen in the difference of the absorption lines on the left and right side in the spectrum. Going from the *a* cut to the *c* cut the areas of the right lines decrease and those of the left lines increase. An important result is the fact that the population does not exceed 50%, so that the ground state is always present as a calibration standard. The number density of anions in *S*I (n_I) normalized to all anions given by $n=n_I+n_{GS}$, called the population $P=n_I/n$, can be determined knowing the Debye-Waller factors. In GS the Debye-Waller factors can be calculated, since we know *n*. Subsequently, in the irradiated sample, the population of GS can be found with the Debye-Waller factors of the unirradiated samples. The Debye-Waller factors of the ground state are not influenced by the coexistence of the metastable state *S*I. Denoting with $t^{G0}=t^{G0}_{1/2}+t^{G0}_{3/2}$ the sum of the effective thickness of the unirradiated sample, with t^{GI} the thickness of the ground state after the irradiation and t^{SI} the thickness of *S*I, we obtain the population from the ratio $t^{GI}/t^{G0}=(n-n_I)/n=1-P$. As pointed out by Carducci,[19] the lattice constants of the crystal should be changed with the population. In order to be independent of this alteration and to get the Debye-Waller factors of *S*I with higher accuracy, we have calculated the ratios $f_i^{SI}/f_i^{GI}=(t^{SI}/P)/(t^{GI}/1-P)$ and $f_i^{SI}/f_i^{G0}=(t^{SI}/P)/(t^{G0}/1-P)$ with $i=a,b,c$. These equations are independent of the crystal thickness. The ratio $t_{1/2}/t_{3/2}$ as a function of Ω in the *a*-*b* plane is given in Fig. 6(a) for pure GS and in Fig. 6(b) for GS and *S*I of the irradiated crystals.

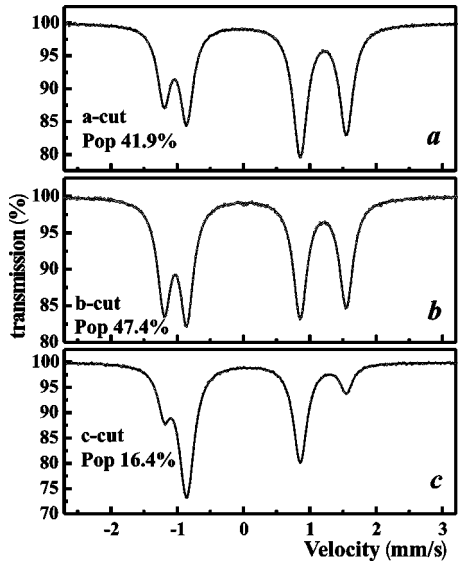

FIG. 5. Mössbauer spectra of the irradiated *a*-, *b*-, and *c*-cut crystals, with perpendicular incidence of the γ quanta to the (100), (010), and (001) faces.

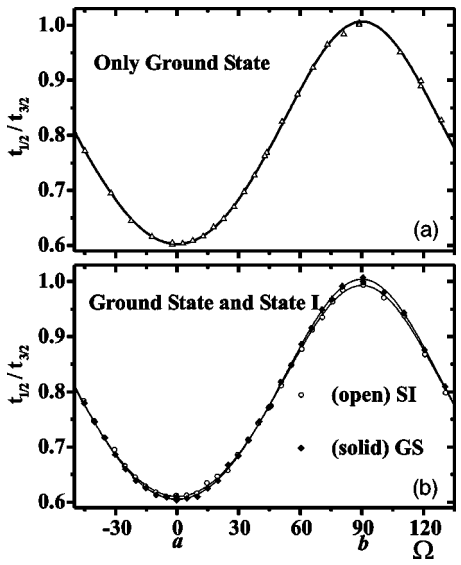

FIG. 6. Dependence of $t_{1/2}/t_{3/2}$ on the rotation angle Ω at $T=80$ K for (a) pure ground state, (b) ground state of the irradiated crystal together with the metastable state *S*I.

All spectra are nearly identical in the ratio of $t_{1/2}/t_{3/2}$. There exists only a very small difference between GS and *S*I in the range of $\mathbf{k}_\gamma \| b$ axis where the values $t_{1/2}/t_{3/2}$ in SI are systematically lower and in the region $\mathbf{k}_\gamma \| a$ axis, where they are systematically a little higher compared to GS. All possible parameters which can be obtained by angle dependent Mössbauer spectroscopy are given in Table II.

It is unambiguously proven that the sign of the EFG is positive in GS and *S*I. The orientation parameter α increases from 35.3 to 35.8° and the main axis of the MSD tensor decreases from 14 to 7°. However, only the increase of α lies significantly outside of the error limit. The asymmetry parameter η decreases inside the error limit. The Debye-Waller factors f_a, f_c increase by 3.1 and 1.6% in *S*I, respectively, and f_b decreases by 1.3% in *S*I. In the ratios Γ_S/Γ_N and Γ_A/Γ_N the line broadening of the source and the line broadening of the absorber in *S*I is considered. We have used two different crystals for the measurement of GS and (GS,

TABLE II. All Mössbauer parameters, the population, the ratio of the linewidths Γ_S/Γ_N, Γ_A/Γ_N, the errors of the crystal preparation $\delta\Omega_a, \delta\Omega_b$, and the ratios of the Debye-Waller factors for *S*I and GS.

	Pure GS	GS	*S*I
sign (q)	+	+	+
α	35.3(1)°	35.4(1)°	35.8(1)°
η	0.021(8)	0.024(8)	0.018(8)
η_c	0.029(9)	0.027(9)	0.010(9)
ω	14(6)°	14(6)°	7(6)°
f_a	0.69(1)	0.58(1)	0.70(1)
f_b	0.66(1)	0.65(1)	0.65(1)
f_c	0.69(1)	0.69(1)	0.70(1)
pop (a) [%]	100	58.1(9)	41.9(9)
pop (b) [%]	100	52.6(9)	47.4(9)
pop (c) [%]	100	83.6(9)	16.4(9)
Γ_S/Γ_N	1.212(9)	1.203(9)	1.203(9)
Γ_G/Γ_N	1	1	1.049(9)
$\delta\Omega_a$	−2.3(6)°	−0.1(6)°	−0.4(6)°
$\delta\Omega_b$	−1.4(6)°	0.5(6)°	0.7(6)°
f ratios (meta/ground):	a	b	c
f^{SI}/f^{G1}	(1.031±0.005)	(0.987±0.005)	(1.016±0.014)

*S*I), which is the reason for the differences in the errors of $\delta\Omega_a$ and $\delta\Omega_b$. The comparison of f_a, f_b, f_c in GS shows that they can be reproduced with an accuracy of about 5%.

V. DISCUSSION

All parameters of GS and *SI* detected by Mössbauer spectroscopy are nearly identical, except QS and IS. Therefore we have to discuss the small changes of the structure and the lattice dynamics, produced, however, by a considerable decrease of the *s*-electron density at the Fe nucleus and a new distribution of the $3d$- and $4p$-electron density, and keeping in mind that *S*I is lying about 1 eV above the ground state. Since the measured rotation spectra show very small deviations from each other, we can assume, in agreement with the results of structure analysis,[11,13,19] that no phase transition of the first or second order occurs by the excitation of *S*I as proposed by Morioca and co-workers.[39,40] Especially the predicted transition from the point symmetry group mmm to mm2 on the basis of probably measured optical activity cannot be confirmed. On the contrary, the discovery of strong isotropic and anisotropic holographic light scattering[41,42] can simply explain the rotation of the polarization of the transmitted light, detectable by an othogonal polarizer with respect to the incoming beam. Consequently, due to the still existing symmetry plane ($Pnnm$) the two different anions 1 and 2 in Fig. 1(c) are equally excited by irradiation with $\mathbf{E}\|$ c axis, which was assumed for our evaluation.

The sign of q is positive in GS and *S*I and q increases in *S*I. Housley[31] has unambiguously demonstrated with magnetic perturbation at $T=297$ K that q is positive, so that in agreement with our results the ratio $t_{1/2}/t_{3/2}$ for $\mathbf{k}_\gamma\|$ a axis is smaller than $t_{1/2}/t_{3/2}$ for $\mathbf{k}_\gamma\|$ b axis. Consequently, the left line in the spectrum at negative velocity is the $\pm 1/2 \rightarrow \pm 1/2$ transition and the right line at positive velocity is the $\pm 1/2 \rightarrow \pm 3/2$ transition. This result is valid in GS and *S*I.

The direction of q is determined by the axial symmetry of the anion, formed by the first coordination sphere C1-Fe-N4 at the central Fe atom. Comparing the angles ϕ_N and ϕ_C with the parameter α, we can propose the relation $\alpha = 1/2(\phi_N + \phi_C)$ for GS. At $T=294$ K the angle α has an amount of $\alpha=35.8°$. From x-ray[24] and neutron data[25] we obtain $\alpha_{x\text{-}ray}=35.9°$ and $\alpha_{neutron}=35.8°$, which is in good agreement with our result. Cooling down to $T=80$ K, ϕ_N and ϕ_C decrease by the same amount to $\alpha_{x\text{-}ray}=35.4°$ (Ref. 13) and $\alpha_{neutron}=35.2°$ (Ref. 11) in comparison of $\alpha = 35.4°$ found by Mössbauer spectroscopy. During crystal cooling the anion rotates by about 0.4° with its C1-Fe-N4 axis towards the a axis. But in *S*I it turns back by about 0.4° to $\alpha=35.8°$. This increase is not in agreement with direct structural methods. It is found in Ref. 11 that α decreases by 0.04°, in Ref. 13 α increases by 0.11°, and in Ref. 19, in which the nitrogen N is replaced by oxygen O, α decreases by 0.21°, which is the worst case, in contradiction to our result. The reason for this discrepancy can be possibly found in the following problems: We can independently determine with Mössbauer spectroscopy the population of *S*I and GS from the effective thicknesses, and we obtain details of the structure from the angle dependence of the cross sections. The structure factor F is determined using x-ray or neutron diffraction, but it consists simultaneously of electron density or nuclear positions of atoms in both states GS and *S*I, e.g., $F=(1-P)\cdot F_{GS}+P\cdot F_{SI}$, whereby F_{GS} and F_{SI} are the structure factors of GS and *S*I and P is the population. Unfortunately, P cannot be determined independently by the intensity of the measured reflexes, it must be taken from other measurements, which opens a large uncertainty, especially if P is introduced into the refinement procedure as a further fit parameter, since F depends linearly on P. The

goodness of the determination of the atomic positions or electron density distribution depends considerably on P. This problem does not exist in Mössbauer spectroscopy.

Considering the asymmetry parameter η, it is clear that due to the small structural asymmetry in the equatorial plane of the anion and the deviation of the Fe-N-O axis from the 180° geometry, η cannot be zero. From the ratio of $\eta^{GS}/\eta^{SI}=(V_{xx}-V_{yy})^{GS}/(V_{xx}-V_{yy})^{SI}\cdot QS^{SI}/QS^{GS}$ we get $(V_{xx}-V_{yy})^{SI}=1.16\cdot(V_{xx}-V_{yy})^{GS}$, so that inside the error limit no asymmetric structural changes occur in the equatorial plane of the anion by excitation of SI. Note that already $\eta_{SI}=0.016$ instead of $\eta_{SI}=0.018$ gives the value of 1.0 instead of 1.16 in the ratio above. With this result we obtain an important view inside the electron density distribution of the $3d_{xz,yz}$ and $4p_{x,y}$ orbitals. Since the $4m$ symmetry is not exactly fulfilled in the anion, the degeneration of the orbitals with e symmetry ($3d_{xz,yz}$ and $4p_{x,y}$) is slightly lifted as given by the following equation:[43]

$$q\cdot\eta=(1-R_{3d})\langle r^{-3}\rangle_{3d}6/7(m3d_{xz}-m3d_{yz}) + (1-R_{4p})\langle r^{-3}\rangle_{4p}6/5(mp_y-mp_x) \qquad (5.1)$$

in which R_{3d}, R_{4p} are the Sternheimer factors[44,45] for the $3d$ and $4p$ electrons, $\langle r^{-3}\rangle_{3d}$ and $\langle r^{-3}\rangle_{4p}$ are the expectation values of r^{-3} of the $3d$ and $4p$ wave functions,[46] and m is the population number of the different orbitals. We cannot calculate m in detail, but using the ratio $q^{GS}\cdot\eta^{GS}/q^{SI}\cdot\eta^{SI}=QS^{GS}\cdot\eta^{GS}/QS^{SI}\cdot\eta^{SI}$, which is unity inside the error limit, we can conclude that the orbital population of the $3d_{xz}$, $3d_{yz}$, $4p_y$, and $4p_z$ orbitals is unaffected in SI, which means that the degeneration is not changed and the symmetry of GS is conserved, provided R_{3d}, R_{4p}, $\langle r^{-3}\rangle_{3d}$, and $\langle r^{-3}\rangle_{4p}$ are constant. However, due to the increase of QS^{SI}, a drastic transfer of electron density between the orbitals $3d_{xz,yz}$ and $3d_{xy}$ or $3d_{z^2}$ and $3d_{x^2-y^2}$ occurs. From differential scanning calorimetry measurements it is known that SI is lying energetically about 1 eV above GS.[7] It is possible that the orbitals Fe($3d_{xz,yz}$) and Fe($3d_{xy}$) are shifted to higher energies. In this case the small degeneracy is unchanged and both orbitals Fe($3d_{xz,yz}$) and Fe($3d_{xy}$) lie at higher energy. Consequently, the possible splitting of the π^*NO orbital can be detected by measuring the charge-transfer transition $3d_{xy}$ or $3d_{xz,yz}\rightarrow\pi^*$NO by absorption spectroscopy.[47] In the ground state the energetic difference between the $6e(3d_{xz,yz})$ and $2b_2(3d_{xy})$ orbitals is about 0.7 eV and the excitation energy between the $2b_2(3d_{xy})$ and the $7e(\pi^*\text{NO})$ orbitals has an amount of about 2.5 eV. These differences are the reason for the temperature independence of QS, detected by Hauser *et al.*[16] Since this result is also valid in SI,[16] the energetic separation of these orbitals must exist in SI, too. In contrast to Tritt-Goc, Pislewski, and Hoffmann[18] no change in the temperature dependence of QS could be found even after an irradiation time of more than 48 h, so that the results of both experiments are in contradiction.

The small increase of the Debye-Waller factors f_a, f_c, and the decrease of f_b as well as the difference of the direction of the MSD main axis with respect to the a axis provide a clear hint that the lattice dynamics is involved going from GS to SI. This observation is confirmed by the detected decrease of all elastic constants in Ref. 48. The population of about 50% of SI leads to a softening of all elastic constants by about 2.5%, compared to GS, so that the phonon spectrum is significantly changed. Therefore it is impossible to use in the refinement procedure of the structure analysis, the ground-state thermal parameters for all atoms (except N and O) in the metastable state SI, as done by Pressprich *et al.*[13] and Carducci, Pressprich, and Coppens.[19] This restriction is very problematic in Ref. 19, where the authors have rotated the N-O ligand,

$$\text{GS:Fe}-\text{N}-\text{O}\rightarrow SI\text{:Fe}-\text{O}-\text{N}, \qquad (5.2)$$

in order to get better thermal parameters for the nitrogen and oxygen atoms. Additionally, Fe is fixed at $T=50$ K to the isotropic ground state value of $U_{iso}=0.003\,16$ Å^2. The isotropic thermal parameter of Fe received from our Mössbauer parameters in GS at $T=80$ K is $U_{iso}=0.0072$ Å^2. The difference by more than a factor of 2 is much too high for a temperature difference of $\Delta T=30$ K. It seems that thermal parameters obtained by least-squares fitting of x-ray data are not useful for such an important assertion of changing N and O. The same problematic situation arises in the determination of the d-orbital population, derived from the Fe multipoles of the electron density maps. Neglecting the $4p$-electron contributions the electric-field gradient, q can be calculated from the equation $q=4/7(1-R_{3d})\langle r^{-3}\rangle_{3d}\cdot\Delta n$, in which $\Delta n=[(nd_{x^2-y^2}-nd_{z^2})+(nd_{xy}-1/2nd_{xz,yz})]$ is the Fe($3d$)-orbital population. Considering only Δn, we get in GS from Ref. 13 $\Delta n=1.66$ and from Ref. 49 $\Delta n=0.84$. These results differ by a factor of 2. Braga, Pavao, and Leite[50] have performed MSXα calculations, receiving $\Delta n=0.45$, from which they have reproduced QS=1.78 mm/s, neglecting R_{3d}. Using $(1-R_{3d})=0.881$ we get QS=1.57 mm/s,[50] QS=2.93 mm/s,[49] and QS=5.79 mm/s.[13] QS of SI cannot be calculated, since in Ref. 13 nd_{xy} is negative and no evaluation is made in the other references. This discussion shows that it is very hard to detect special features of the electron density on the Fe-central atom from x-ray analysis and multipole refinement. From our Mössbauer results we cannot confirm the rotation of the N-O ligand to Fe-O-N. A strong hint of this structural modification is given by density-functional calculation,[20] with which a stable Fe-O-N configuration reproduces the Mössbauer parameters QS, IS, η of GS, and SI with an uncertainity of about 5%.

In conclusion, from the nearly identical Mössbauer parameters α, η, ω, f_a, f_b, f_c in the ground and metastable state SI we assume that the charge in the range of the Fe-N-O quasifourfold axis is rearranged in SI and as shown in Ref. 11 the atomic distances Fe-N and N-O are somewhat elongated. But the symmetry of the $[\text{Fe}(\text{CN})_5\text{NO}]^{2-}$ anion and that of the crystal are unaffected by the population of SI. The space group $Pnnm$ is present in both states GS and SI. Due to these results we have proposed that SI has the same electronic configuration as GS, formally $6e(3d_{xy,yz})^4$, $2b_2(3d_{xy})^2$, and $7e(\pi^*\text{NO})^0$, only the $2b_2$ orbital or probably the $6e$ and $2b_2$ orbitals are shifted to higher energies, whereby an exchange of electron density between these orbitals are possible, which can explain the larger QS and more positive IS in SI. Unfortunately, we cannot clearly decide with Mössbauer spectroscopy between the proposed two configurations Fe-N-O and Fe-O-N. This

open question will be resolved by infrared and Raman spectroscopy using isotopic substitution of the oxygen and nitrogen.

ACKNOWLEDGMENTS

This work was supported by the Deutsche Forschungsgemeinschaft project Wo 618/1-2 and by the DAAD. V. Angelov is very indebted to the DAAD for his stay in Cologne.

APPENDIX

1. Evaluation of the measured spectra

Every single spectrum was fitted by the transmission integral procedure. The shape of the spectrum obtained with a single line, emitted from the source, without any polarization effect is given by

$$N(n)=N_\infty[1-\beta\cdot T(n)], \tag{A1}$$

where $N(n)$ is the number of counts in channel n, β is the recoilless fraction, and $T(n)$ is the transmission integral:

$$T(n)=\frac{1}{\pi}\int_{-\infty}^{\infty}\frac{1-\exp(-A)}{(x-n)^2+(\Gamma_S/2)}\,\frac{\Gamma_S}{2}\,dx. \tag{A2}$$

Here A is given for the quadrupole splitting of SNP by

$$A=\frac{\Gamma_N\Gamma_A t_{1/2}/4}{\Gamma_A^2/4+(E-P_{1/2})^2}+\frac{\Gamma_N\Gamma_A t_{3/2}/4}{\Gamma_A^2/4+(E-P_{3/2})^2}. \tag{A3}$$

E is the energy and $P_{1/2}$ and $P_{3/2}$ are the positions of the two lines. In the case of an unpolarized source but polarized absorption with diagonal Σ matrix it is necessary to introduce an effective thickness for each polarization 1,2 and $i=1/2,\ 3/2$:

$$t_{i1}=t_i(1-a_i),\quad t_{i2}=t_i(1+a_i), \tag{A4}$$

$$t_i=(t_{i1}+t_{i2})/2,\quad a_i=\frac{t_{i2}-i_{i1}}{t_{i1}+t_{i2}}. \tag{A5}$$

Therefore in this case the experimental spectrum is given by a sum of two transmission integrals due to the two polarizations 1,2:

$$N(n)=N_\infty\left[1-\beta\frac{T_1(n)+T_2(n)}{2}\right]. \tag{A6}$$

In GS the linewidth Γ_A is exactly Γ_N and in *SI* the small line broadening[37] has been taken into account.

2. Iteration algorithm

The self-consistent iteration algorithm, which is used for the determination of $\alpha,\eta,\omega,f_a,f_b,f_c$ and the fractional polarizations $a_{1/2},a_{3/2}$, is calculated in the following steps: After reading of all data for each spectrum, the fractional polarizations are set to 0. The effective thicknesses $t_{1/2}$, $t_{3/2}$ and their errors are calculated from the transmission integral. The ratios $t_{1/2}/t_{3/2}$ are fitted to Eqs. (3.12) or (3.27), obtaining the unknown parameters α,η,G_o and the errors of the crystal orientation $\delta\Omega_a,\delta\Omega_b$. With these parameters the polarizations $a_{1/2},a_{3/2}$ are calculated, fitting again $t_{1/2}/t_{3/2}$ to Eqs. (3.12) or (3.27) obtaining new values of α,η,G_o as long as the corrections are sufficiently small. In the last step we have calculated the Debye-Waller factors f_a, f_b, f_c, and ω. We need about three iteration cycles with this procedure to reveal a stable configuration of all parameters.

[1] Th. Woike, W. Kirchner, G. Schetter, Th. Barthel, H. Kim, and S. Haussühl, Opt. Commun. **106**, 6 (1994).

[2] S. Haussühl, G. Schetter, and Th. Woike, Opt. Commun. **114**, 219 (1995).

[3] Th. Woike, S. Haussühl, B. Sugg, R. A. Rupp, J. Beckers, M. Imlau, and R. Schieder, Appl. Phys. B: Lasers Opt. **63**, 243 (1996).

[4] M. Imlau, S. Haussühl, Th. Woike, R. Schieder, V. Angelov, R. A. Rupp, and K. Schwarz, Appl. Phys. B: Lasers Opt. **68**, 877 (1999).

[5] U. Hauser, V. Oestreich, and H. D. Rohrweck, Z. Phys. A **280**, 17 (1977); **280**, 125 (1977).

[6] J. J. Spijkerman, F. C. Ruegg, and J. R. DeVoe, Tech. Rep. Ser. I. A. E. A. **50**, 254 (1966).

[7] Th. Woike, W. Krasser, H. Zöllner, W. Kirchner, and S. Haussühl, Z. Phys. D: At., Mol. Clusters **25**, 351 (1993).

[8] Th. Woike, H. Zöllner, W. Krasser, and S. Haussühl, Solid State Commun. **73**, 149 (1990).

[9] Th. Woike and S. Haussühl, Solid State Commun. **86**, 333 (1993).

[10] K. Ookubo, Y. Morioka, H. Tomizawa, and E. Miki, J. Mol. Struct. **379**, 241 (1996).

[11] M. Rüdlinger, J. Schefer, G. Chevrier, N. Furer, H. U. Güdel, S. Haussühl, G. Heger, P. Schweiss, T. Vogt, Th. Woike, and H. Zöllner, Z. Phys. B: Condens. Matter **83**, 125 (1991).

[12] M. R. Pressprich, M. A. White, and P. Coppens, J. Am. Chem. Soc. **115**, 6444 (1993).

[13] M. R. Pressprich, M. A. White, Y. Vekhter, and P. Coppens, J. Am. Chem. Soc. **116**, 5233 (1994).

[14] B. Elschner and G. Kruschel (private communication); G. Kruschel, diploma thesis, Darmstadt, 1988.

[15] C. Terrile, O. R. Nascimento, I. J. Moraes, E. E. Castellano, O. E. Piro, and J. A. Aymonino, Solid State Commun. **73**, 481 (1990).

[16] U. Hauser, M. Klimm, L. Reder, T. Schmitz, M. Wessel, and H. Zellmer, Phys. Lett. A **144**, 39 (1990).

[17] H. U. Güdel, Chem. Phys. Lett. **175**, 262 (1990).

[18] J. Tritt-Goc, N. Pislewski, and S. K. Hoffmann, Chem. Phys. Lett. **268**, 471 (1997).

[19] M. D. Carducci, M. R. Pressprich, and P. Coppens, J. Am. Chem. Soc. **119**, 2669 (1997).

[20] B. Delley, J. Schefer, and Th. Woike, J. Chem. Phys. **107**, 10 067 (1997).

[21] V. Angelov, R. Rusanov, Ts. Bonchev, Th. Woike, and S. Haussühl, Z. Phys. B **83**, 39 (1991).

[22] J. Stevens and V. Stevens, *Mössbauer Effect Data Index 1974*,

(Plenum Press, New York, 1975).
[23] P. T. Manoharan and W. C. Hamilton, Inorg. Chem. **2**, 1043 (1963).
[24] F. Bottomley and P. S. White, Acta Crystallogr., Sect. B: Struct. Crystallogr. Cryst. Chem. **35**, 2193 (1979).
[25] A. Navaza, G. Chevrier, P. M. Alzari, and P. J. Aymonino, Acta Crystallogr., Sect. C: Cryst. Struct. Commun. **45**, 839 (1989).
[26] M. Y. Antipin, V. G. Tsirelson, M. P. Flyugge, Y. T. Struchkov, and R. P. Ozerov, Sov. J. Coord. Chem. **13**, 67 (1987).
[27] V. Rusanov, V. Angelov, J. Angelova, Ts. Bonchev, Th Woike, H. Kim, and S. Haussühl, Solid State Commun. **123**, 39 (1996).
[28] Ph. Dufek, P. Blaha, and K. Schwarz, Phys. Rev. Lett. **75**, 3545 (1995).
[29] R. M. Housley, R. W. Grant, and U. Gonser, Phys. Rev. **178**, 514 (1969).
[30] R. W. Grant, R. M. Housley, and U. Gonser, Phys. Rev. **178**, 523 (1969).
[31] R. M. Housley, in *Mössbauer Effect Methodology*, edited by I. J. Gruverman (Plenum Press, New York, 1970), Vol. 5.
[32] T. C. Gibb, Chem. Phys. Lett. **30**, 137 (1975).
[33] T. C. Gibb, J. Chem. Soc. Dalton Trans. **1978**, 743.
[34] R. Zimmermann and R. Doerfler, Hyperfine Interact. **12**, 79 (1982).
[35] H. Spiering, in *Mössbauer Spectroscopy Applied to Inorganic Chemistry*, edited by Gary J. Long (Plenum Press, New York, 1984), Vol. I.
[36] Vissscher (private communication).
[37] Th. Woike, W. Kirchner, H. Kim, S. Haussühl, V. Rusanov, V. Angelov, S. Ormandjiev, and Ts. Bonchev, Hyperfine Interact. **77**, 265 (1993).
[38] P. Steiner, E. Gerdau, H. Hautsch, and D. Steenken, Z. Phys. **221**, 281 (1969).
[39] Y. Morioka, Solid State Commun. **82**, 505 (1992).
[40] Y. Morioka, Spectrochim. Acta A **50**, 1499 (1994).
[41] M. Imlau, Th. Woike, R. Schieder, and R.A. Rupp, Phys. Rev. Lett. **82**, 2860 (1999).
[42] M. Imlau, R. Schieder, R.A. Rupp, and Th. Woike, Appl. Phys. Lett. **75**, 16 (1999).
[43] A. Vértes, L. Korecz, and K. Burger, *Mössbauer Spectroscopy: Studies in Physical and Theoretical Chemistry 5* (Elsevier Scientific Publishing Company, New York, 1979).
[44] R. M. Sternheimer, Phys. Rev. **105**, 158 (1957).
[45] Z. Su and P. Coppens, Acta Crystallogr., Sect. A: Found. Crystallogr. **A52**, 748 (1996).
[46] D. M. S. Esquivel, D. Guenzburger, and J. Danon, Phys. Rev. B **19**, 1357 (1979).
[47] W. Krasser, Th. Woike, S. Haussühl, J. Kuhl, and A. Breitschwerdt, J. Raman Spectrosc. **17**, 83 (1986).
[48] K. Lüghausen, H. Siegert, Th. Woike, and S. Haussühl, J. Phys. Chem. Solids **56**, 1291 (1995).
[49] R. Bolotovski, A. Darovski, V. Kezerashvili, and P. Coppens, J. Synchrotron Radiat. **2**, 181 (1995).
[50] M. Braga, A. C. Pavao, and J. R. Leite, Phys. Rev. B **23**, 4328 (1981).